 CMES, vol.21, no.1, pp.81-91, 2007

A Hyperelastic Description of Single Wall Carbon Nanotubes at Moderate Strains and Temperatures

Xianwu Ling[1] **and S.N. Atluri**[1]

Abstract: In this work, single wall carbon nanotubes (SWNTs) are shown to obey a hyperelastic constitutive model at moderate strains and temperatures. We consider the finite temperature effect via the local harmonic approach. The equilibrium configurations were obtained by minimizing the Helmholtz free energy of a representative atom in an atom-based cell model. We show that the strain energy can be fitted by two cubic polynomials, which consequently produces for the linear elasticity a linearly increasing tangent modulus below a critical strain and an almost linearly decreasing tangent modulus beyond the critical strain. To avoid the strain dependent tangent modulus, we propose to use Ogden's hyperelasticity model to describe the mechanical behaviors of SWNTs. Our results indicate a constant μ for Ogden's hyperelastic model for moderately large strains for large tubes and below 900°K. The armchair tubes are shown to be much stronger and stiffer, but less ductile than the zigzag tubes. We also show that small tubes are more ductile but less stronger. Small tubes and high temperatures reveal more nonlinearity.

1 Introduction

The exceptional mechanical properties of carbon nanotubes (CNTs) have aroused intense research interest. Single wall carbon nanotubes (SWNTs) possess extremely high stiffness (in the range of TPa), strength (in the range of GPa) and resilience (of 4-15% strain), which are far beyond the nearest computing materials (say, steel) with their properties in the range of GPa, MPa and $10^{-6} \sim 10^{-4}$ strains. Together with their relatively low densities ($\sim 1/3$ of steel), CNTs are contemplated as a great promise for reinforcement materials of next generation composites. But a clear understanding of their mechanical properties is essential for unlocking this potential.

Knowledge of their mechanical properties is the first step towards the rational application of CNTs as structural elements. Linear elasticity has been the tool used to derive the Young's modulus for the CNTs since their discovery. However, a very large scatter exists for the reported elastic Young's modulus (Y), with a wide spread of data over one order in magnitude. In Table 1, we summarize a collection of experimental and theoretical Young's moduli, among many others that cannot be listed here. Experimental measurements are difficult and involve many uncertainties, such as the structural uncertainty (e.g., as caused by defect), the measurement uncertainty (e.g., as caused by thermal vibration), and the model uncertainty (e.g., as caused by the elastic beam or shell assumption). Hence, experimental errors are generally very high. Computational modeling provides a powerful tool to confirm, supplement and guide experimental researches. Theoretical investigations have involved calculations from the first principle Hartree-Fock method through the empirical potential molecular mechanics (MM) and molecular dynamics (MD) to the elastic continuum-based models. Nevertheless, no agreements in the predicted Young's modulus can be made.

The high stiffness reported not only provide a significant enhancement over existing materials, but also result in unusual high strengths of CNTs. The strengths of CNTs are much less studied than their stiffness. Wong et al. (1997) measured the bending strength of large diameter MWNTs in the

[1] Center for Aerospace Research and Education, University of California at Irvine, 5251 California Ave., Suite 140, Irvine, CA 92612

Table 1: Reported Young's modulus (TPa)

Ref.	Method	Value	Note
Treacy, Ebbesen, and Gibson (1996)	Experiment (TEM)	$1.85^{+1.65}_{-1.45}$	MWNTs[1]
Wong, Sheehan, and Lieber (1997)	Experiment (AFM)	$0.69-1.87$	MWNTs
Lourie and Wagner (1998)	R. Spectroscopy	$2.8-3.6$ $1.7-2.4$	SWNTs MWNTs
Krishnan, Dujardin, Ebbesen, Yianilos, and Treacy (1998); Demczyk, Wang, Cumings, Hetman, Han, Zettl, and Ritchie (2002)	Experiment (TEM)	$1.25^{+.45}_{-.35}$	SWNTs
Salvetat, Briggs, Bonard, Bacsa, Kulik, Stöckli, Burnham, and Forró (1999)	Experiment (AFM)	$0.06-1.3$	Ropes
Tombler, Zhou, Alexseyev, Kong, Dai, Liu, Jayanthi, Tang, and Wu (2000)	Experiment (AFM)	1.2	SWNTs
Yu, Files, Arepalli, and Ruoff (2000); Yu, Lourie, Dyer, Moloni, Kelly, and Ruoff (2000)	Experiment (AFM)	$0.27-0.95$	MWNTs
Yakobson, Brabec, and Bernholc (1996); Gao, Cagin, and Goddard (1998)	MD	5.5; 0.64	SWNTs[2]
Cornwell and Wille (1997)	Quenched MD	$0.2-2.0$	(n,n)
Lu (1997)	Force constant	$0.97-1.11$	CNTs
Halicioglu (1998)	MD	$0.44-0.50$	SWNTs
Hernández, Goze, Bernier, and Rubio (1998); Ozaki, Iwasa, and Mitani (2000)	Tight binding	1.24; 0.98	CNTs
Yao and Lordi (1998); Popov, Van Doren, and Balkanski (2000)	Lattice Dyn.	~ 1	SWNTs
Van Lier, Van Alsenoy, Van Doren, and Geerlings (2000)	Hartree-Fock	0.72-1.12	SWNTs
Zhou, Duan, and Gu (2001)	LDA	0.764	SWNTs
Belytschko, Xiao, Schatz, and Ruoff (2002)	Modified Morse	0.94	CNTs
Sears and Batra (2004)	Molecular Mech.	0.99	CNTs

1. first measurement; 2. Yakobson (1996) used $h = 0.066$.

range of 14.2 ± 0.8 *GPa*. Wanger et al. (1998) reported a tensile strength of 55 GPa by directly observing fragmentation of a SWNT in a polymer matrix. Walters et al. (1999) estimated the tensile strength to be 45 ± 7 *GPa* for CNT bundles. Pan et al. (1999) measured the tensile strength of a very long ($\sim 2mm$) ropes to be 1.72 ± 0.64 *GPa*. The low strength values measured were attributed to defect concentration in their specimens. Li et al. (2000) fit the tensile strength of SWNTs to be ~ 22 *GPa*. Theoretical prediction (MD) of CNT strengths has emphasized more on the role of the defects and will not be covered here.

Although the linear elasticity modeling of CNTs is ubiquitous in the literature, several authors also noticed the nonlinearity of the CNTs. Yao et al. (1998) indicated the strain effects on the Young's modulus in their MD simulations. Xiao et al. (2002,2004) fit the strain energy change of CNTs with a cubic function, from which they deduced a linearly strain-dependent in-plane stiffness. Arroyo and Belytschko (2004) proposed a finite deformation nonlinear elastic theory based on the interatomic potentials. Natsuki and Endo (2005) presented a structural mechanics approach based on molecular mechanics and made similar observations as Xiao and Liao (2002).

The present work aims to provide a hyperelastic

constitutive model to describe the mechanical behaviors of SWNTs. Although Xiao et al. (2002) and Natsuki et al. (2005) described the CNTs stiffness with a linearly strain-dependent function, instead of a singly strain-independent value prevalent in the literature, they still implicitly assumed the linear elasticity model. In this work, instead of a strain-dependent Young's modulus using linear elasticity, we show that in CNTs, the strain energy cannot be represented by a simple quadratic function of the uniaxial strain. We then use Ogden's hyperelasticity model [Ogden, (1984)] (which is essentially a quadratic function of the principal stretches), from which a constant material parameter is obtained for temperatures up to 900°K.

2 Atom-based cell model

The atom-based cell model is presented in Ling and Atluri (2006) and illustrated in Figure 1, where the representative atom A is surrounded by three nearest neighbor atoms B, C and D, forming a lattice cell. The atoms interact through the Tersoff-Brenner potential [Brenner (1990)]. The polar coordinate system is used to describe the positions of the atoms, in which A is positioned at $(r,0,0)$ and $\varphi_i = cos^{-1}x_i/r$ for $i = B$, C, D. The second nearest neighbor atoms are determined using the nearest neighbor atom coordinates. For instance, the equivalence of bond $BB1$ and CA yields

$$\varphi_{B1} = \varphi_B + (\varphi_A - \varphi_C) = \varphi_B - \varphi_C, \tag{1}$$

$$z_{B1} = z_B + (z_A - z_C) = z_B - z_C. \tag{2}$$

Similarly, the positions of B2, C1, C2, D1, D2 can be derived.

SWNTs can be imagined as a rolled graphene sheet, which, upon unrolling is illustrated in Figure 1(b). The unrolled sheet can be visualized by cutting the SWNT along its axial direction followed by unrolling it *without* stretching to the tangent plane at A. In the planar graphene, we set a 2D Cartesian coordinate system such that $x_A = 0$, $y_A = 0$. Then, the positions of the nearest neighbor atoms in the 2D Cartesian system are given by $(r\varphi_i, z_i)$, where $i = B,C,D$. The graphene

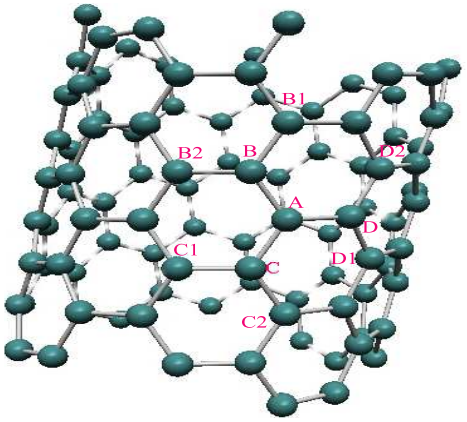

(a) Rolled

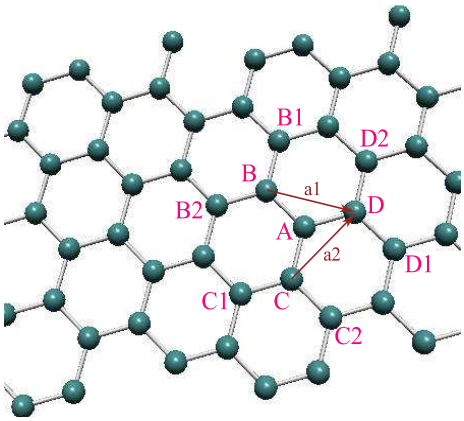

(b) Planar

Figure 1: Cell model of an SWNT in the rolled and planar forms.

basis vectors $\mathbf{a}_1$ and $\mathbf{a}_2$ are now given by

$$\mathbf{a}_1 = \overrightarrow{BD} = [r(\varphi_D - \varphi_B), z_D - z_B], \tag{3}$$

$$\mathbf{a}_2 = \overrightarrow{CD} = [r(\varphi_D - \varphi_C), z_D - z_C]. \tag{4}$$

The rolling opertation is performed in such a way that a graphene lattice vector $\mathbf{c} = n\mathbf{a}_1 + m\mathbf{a}_2$ becomes the circumstance of the tube, where the chirality (n,m) uniquely determines the tube. Utilizing the equations (3) and (4), the circumstance of the tube is now given by

$$\begin{aligned} |\mathbf{c}| &= \sqrt{\mathbf{c}\cdot\mathbf{c}} \\ &= \sqrt{(r^2 sq_1 + sq_2)} \end{aligned} \tag{5}$$

in which,

$$sq_1 = [n(\varphi_D - \varphi_B) + m(\varphi_D - \varphi_C)]^2$$

$$sq_2 = [n(z_D - z_B) + m(z_D - z_C)]^2$$

Meanwhile,

$$|\mathbf{c}| = 2\pi r. \tag{6}$$

Equations (5) and (6) yield

$$\begin{aligned} g =& r^2\left([n(\varphi_D-\varphi_B)+m(\varphi_D-\varphi_C)]^2-4\pi^2\right) \\ &+[n(z_D-z_B)+m(z_D-z_C)]^2\equiv 0, \end{aligned} \tag{7}$$

where g is a geometric constraint that connects the tube chirality to the coordinate variables.

The finite temperature effect is accounted for by the Helmholtz free energy H, which, via the local harmonic approach [LeSar et al. (1989)], is expressed as

$$H = U_{tot} + k_B T \sum_{i=1}^{N}\sum_{\kappa=1}^{3} \ln\left[2\sinh\left(\frac{h\omega_{i\kappa}}{4k_B T}\right)\right], \tag{8}$$

where U_{tot} is the total potential energy and N is the total number atoms. The atom vibrating frequencies $\omega_{i\kappa}$ are given by

$$\left|\omega_{i\kappa}^2\mathbf{I}_{3\times 3} - \frac{1}{m_C}\frac{\partial^2 U_{tot}}{\partial \mathbf{x}_i \partial \mathbf{x}_i}\right| = 0, \quad i = 1,2,\ldots N. \tag{9}$$

For an SWNT, the frequencies $\omega_{i\kappa}$ are independent of the atom i and thus taken as $\omega_{A\kappa}$. To solve for $\omega_{A\kappa}$, U_{tot} is partitioned into two parts, i.e., those bonds of the first closest layers, i.e., AB, AC, AD, and through the bond angles in those of the second closet layers, i.e., $BB1, BB1, CC1, CC2, DD1, DD2$. Therefore, the total energy can be expressed as

$$\begin{aligned} U_{tot} =& V_{AB}+V_{AC}+V_{AD} \\ &+V_{BB1}+V_{BB2}+V_{CC1}+V_{CC2}+V_{DD1}+V_{DD2} \\ &+\text{bond energies independent of atom } A. \end{aligned} \tag{10}$$

Equations (9) and (10) define $\omega_{A\kappa}$ in terms of the coordinate variables.

For the Tersoff-Brenner formalism, the total potential energy U_{tot} can also be expressed as

$$U_{tot} = \frac{1}{2}\sum_i\sum_{j\neq i} V_{ij} = NU_a, \tag{11}$$

where $U_a = \frac{1}{2}(V_{AB}+V_{AC}+V_{AD})$ is the potential energy per atom. Therefore, the Helmholtz free energy per atom H_a is obtained as

$$H_a = U_a + k_B T \sum_{\kappa=1}^{3} \ln\left[2\sinh\left(\frac{h\omega_{A\kappa}}{4k_b T}\right)\right]. \tag{12}$$

Since both U_a and $\omega_{A\kappa}$ are implicit functions of the coordinate variables (r, φ_i, z_i) for $i = B,\ C.\ D$, the equilibrium atom positions are obtained by minimizing H_a, i.e.:

$$\frac{\partial H_a}{\partial r} = 0,\ \frac{\partial H_a}{\partial \varphi_i} = 0,\ \frac{\partial H_a}{\partial z_i} = 0, \text{ for } i = B,C,D, \tag{13}$$

subjected to the nonlinear chirality constraint $g \equiv 0$.

The uniaxial tension is imposed by enforcing that

$$Z_B - Z_C = \lambda_z l_0, \quad \text{provided} \quad Z_B \geq Z_D, \tag{14}$$

where ε_z and $\lambda_z = \exp(\varepsilon_z)$ are respectively the axial strain and stretch, and $l_0 = Z_{B0} - Z_{C0}$ is the initial z-axis length. As cab be seen, equation (14) provides a straightforward means to applying the Cauchy-Born rule Born and Huang (1954) to the non-centrosymmetric atomic structures.

3 Results and discussion

The strain energy E is stored in the form of the carbon bond energy and atom vibration. Hence, we set

$$E = \Delta H_a / V_0, \tag{15}$$

where the change of the free energy

$$\Delta H_a = H_a - H_{a0}, \tag{16}$$

and where H_{a0} is the reference free energy at $\varepsilon_z = 0$, and V_0 is the volume per atom in the undeformed configuration. Figure 2 compares the strain energy versus the applied strains from several sources. Impressively, our computed ΔH_a's perfectly match the MD results by Cornwell et al. (1997) and the structural mechanics results by Natsuki et al. (2005). For small strains, the

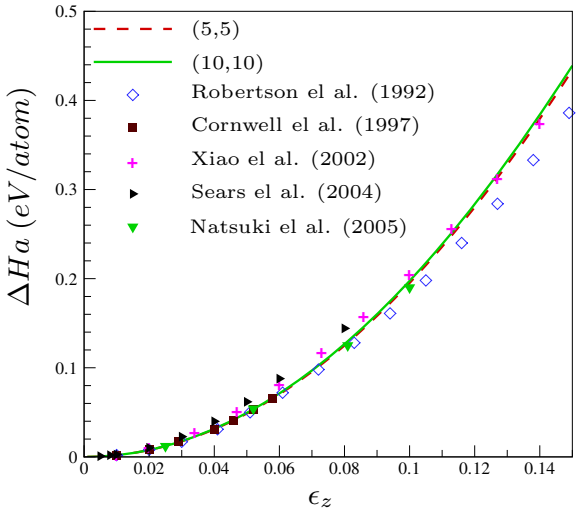

Figure 2: Energy change per atom under axial tension. Note that (1) the present results for (10,10) and (5,5) tubules are at $T = 300^{o}$K; (2) Robertson el al's results are picked from their Tersoff-Brenner potential calculations; (3) Cornwell et al's results are picked from their results for (9,9) tube; (4) Sears el al's results are also picked from their Tersoff-Brenner potential calculations. If their MM3 potential results are picked instead, a much better agreement is obtained.

present results also match very well the MD results by Robertson et al. (1992) and the MM results by Sears et al. (2004). The overall deviations are also small for the MD results by Xiao et al. (2002). Similar to Cornwell et al. (1997), the tube radius is seen to have a negligible effect on the strain energy. In our calculations, the temperature effect on the strain energy is slight, e.g., the strain energy at $\varepsilon = 0.15$ decreases by less than 4% from $T = 150$ to $T = 900^{o}$K, and for smaller strains, even smaller changes incur. We mention that the results by other researchers were reported only for absolute zero temperature.

As noticed by Xiao et al. (2002), the strain energy can be fitted by a cubic polynomial as

$$E = a_2\varepsilon_z^2 + a_3\varepsilon_z^3, \tag{17}$$

where the coefficients of a_2, a_3 are determined by a regression analysis. For the SWNT (10,10) at 300^{o}K, we obtain $a_2 = 20.10$ and $a_3 = -3.38eV/atom$, with a standard deviation less than 3.28×10^{-4} for strain up to 0.15. Xiao et al. (2002) estimated $a_2 = 25.6$, $a_3 = -48.2$ in their simulations with a standard deviation of 0.005. Although the overall standard deviation is very small, we note that the deviation is nearly totally contributed from the fitted data for small strains up to 0.04. Therefore, we divide the fitting into two regions and obtain $a_2 = 19.45$, $a3 = 6.15$ with a standard error 2×10^{-6} for strains up to 0.04, and $a2 = 20.12$, $a3 = -3.78$ with a standard error of 3.53×10^{-4} for strains in between 0.04 and 0.15. The initial stiffness estimations of a_2 match quantitatively in all the cases. However, the initial increase and the subsequent decrease of the stiffness cannot be captured by the whole region regression as Xiao et al. (2002) did. The present results also predict a smaller nonlinear coefficient a_3. The fact is that E is not a perfect quadratic function in ε_z, which clearly indicates that the SWNT is hyperelastic and cannot be simply described by linear elasticity.

Under uniaxial tension, we define the tangent modulus for uniaxial stiffness as

$$Y = \frac{\partial^2 E}{\partial \varepsilon_z^2} = \frac{1}{V_0}\frac{\partial^2 H_a}{\partial \varepsilon_z^2}. \tag{18}$$

Y was generally regarded as the Young's modulus in prior literature, often with its single value evaluated at $\varepsilon_z = 0$. The central finite difference scheme is employed to calculate the second derivative of E. An important quantity in determined the elastic properties is the wall thickness h as imbedded in V_0. To the best knowledge of the authors, a common estimate of the SWNT thickness is $h \equiv 0.34nm$–the interlayer distance of graphite, although Yakobson et al. (1996) calculated $h = 0.066nm$. We use the constant wall thickness $h = 0.34nm$ in our calculations. Nevertheless, a different value of h only affects the tangent modulus by a constant factor. Figure 3 shows that Y can be well characterized by a linear function of ε_z before when it drops at a critical strain, in excellent agreement with the two stage fitting of the strain energy. But the strain dependence of Y puts ambiguity into its conventional understanding as the Young's modulus. Nevertheless, we note that (1) Y is of the order of 1 TPa for the armchair CNTs, but nearly reduced by half for

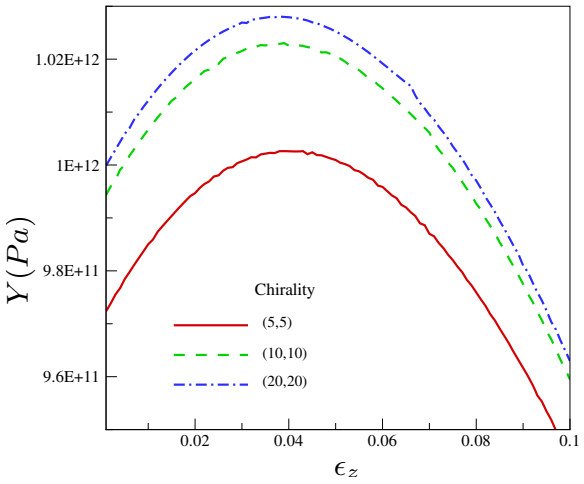

(a) Armchair

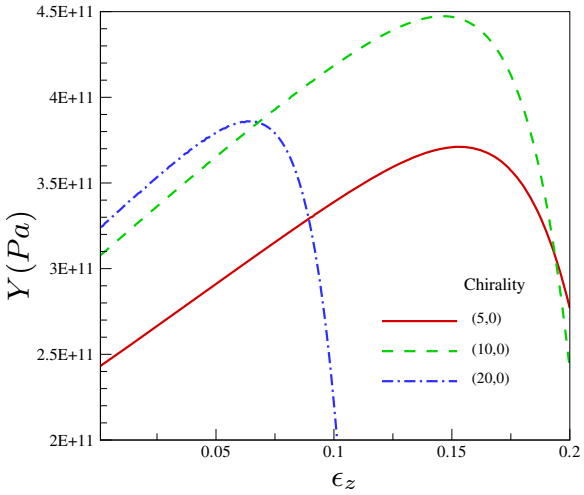

(b) Zigzag

Figure 3: Predicted tangent modulus for SWNTs at 300°K.

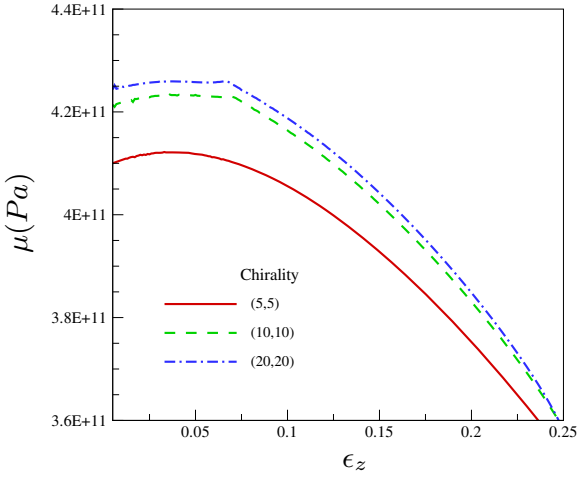

(a) Armchair

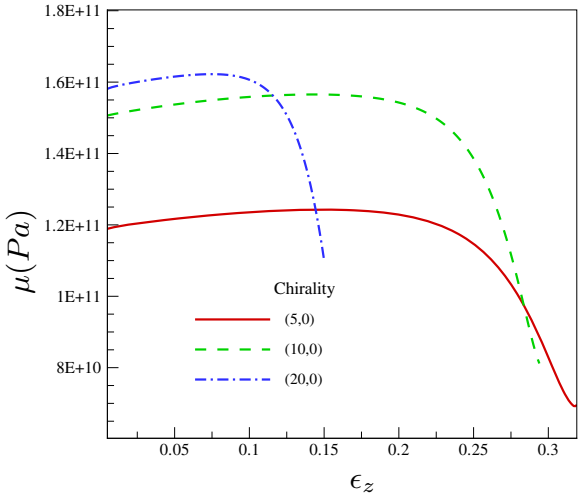

(b) Zigzag

Figure 4: Predicted μ for Ogden's hyperelasticity model.

the zigzag tubes; (2) large tubes have greater stiffness than the small tubes. No agreement on the size effect on the Young's modulus has been observed [c.f., Lu (1997), Hernández (1998), Yao and Lordi (1998)]; and (3) the critical strain at which Y drops is nearly $4 \sim 6\%$ strain for the armchair tubes, but $10 \sim 20\%$ strain for the zigzag tubes (with the larger tubes failing earlier).

While equation (17) indicates the hyperelasticity behavior of SWNTs, it does not provide a strain energy density function under general deformation. Ogden (1984) derived the strain energy density function for a hyperelastic material as

$$E = \frac{1}{2}\mu\left(\lambda_z^2+\lambda_\theta^2+\lambda_r^2-3-2\ln J\right) + \frac{1}{2}\mu'(J-1)^2, \quad (19)$$

where $J=\lambda_z\lambda_\theta\lambda_r$ is the Jacobian of deformation (with λ_θ, λ_r being respectively the stretches in the hoop and thickness directions, and as noted earlier, $\lambda_z = \exp(\varepsilon_z)$). Since the SWNT consists only a single layer of atoms,

$$\hat{\sigma}_r = \lambda_r \frac{\partial E}{\partial \lambda_r} \equiv 0, \quad (20)$$

where $\hat{\sigma}_r$ is the radial Kirchhoff stress. Equations (19-20) yield

$$\mu' = \frac{1-\lambda_r^2}{J(J-1)}\mu \equiv 0, \tag{21}$$

using $\lambda_r \equiv 1$. Thus,

$$\mu = \frac{2E}{\lambda_z^2+\lambda_\theta^2-2-2\ln J}. \tag{22}$$

Figure 4 shows the calculated μ for Ogden's hyperelasticity model at 300°K. A nearly constant μ is observed for all the tubes below the critical strains of 4-6% for armchair tubes and of 10-20% for zigzag tubes, though each tube has its own μ value. The nonlinearity becomes more obvious for small tubes, as μ becomes more dependent on the applied strains. This is understandable since in small tubes, the out-of-plane π-bonds become more severely distorted. The critical strain can be clearly read from the curves for two large armchair tubes (20,20) and (10,10), which take a sharp turn at 0.065 and 0.07 strain, respectively. It is noticed that the deformation of an SWNT is completely reversible (i.e., elastic) subjected to strains of more than 4% [Yakobson et al.(1996), Wong et al. (1997), Lourie et al. (1998)]. Also in accordance with Nardelli et al. (1998) and Zhang et al. (1998), the zigzag tubes display a higher strain resilience. Hence, the critical strain from our simulations can possibly indicate the elastic limit. The present cell model cannot be used beyond the elastic limit as it does not consider the Stone-Wales transformation.

The temperature effect on the predicted μ is plotted in Figure 5 for the armchair tube (10,10). μ decreases with increasing temperatures, and the higher the temperature, the greater the decrease. At high temperatures, no apparent elastic stage can be recognized, as even μ becomes strain dependent. Our observation is consistent with the latest discovery of superplastic CNTs at high temperature by Huang et al. (2006).

Now, we look at the stress predictions. For the linear elasticity model, the tensile stress is given by

$$\sigma_z = \frac{\partial E}{\partial \varepsilon_z} = \frac{1}{V_0}\frac{\partial H_a}{\partial \varepsilon_z}. \tag{23}$$

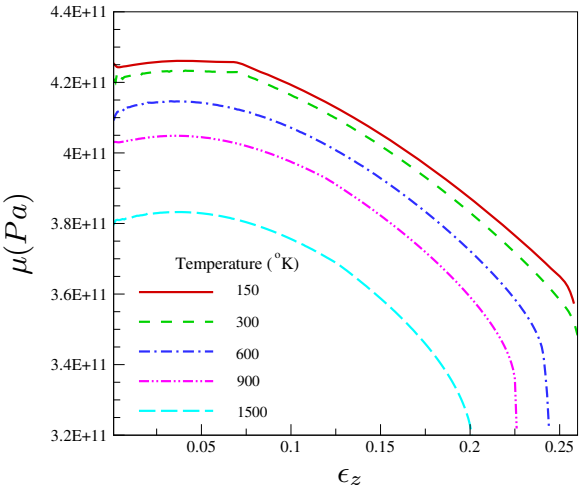

Figure 5: Temperature effect on μ.

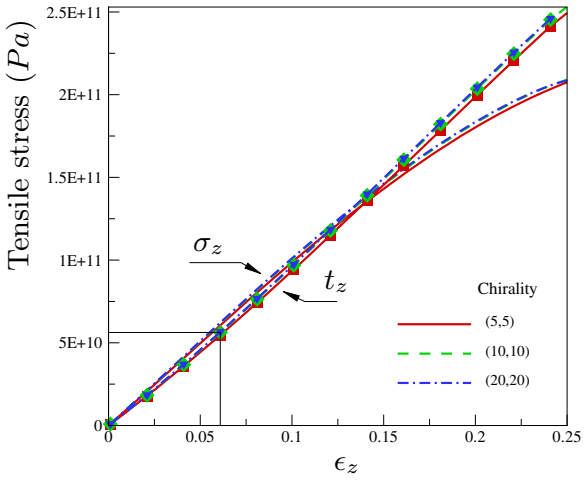

Figure 6: Tensile stresses prediction by the linear elasticity model and the hyperelasticity model. The lines with symbols are from Ogden's model. Armchair tubes.

For Odgen's hyperelasticity model, the axial Cauchy stress is defined as

$$t_z = \frac{\lambda_z}{J}\frac{\partial E}{\partial \lambda_z}, \tag{24}$$

which, upon substituting equation (19), yields

$$t_z = \frac{\mu}{\lambda_\theta V_0}\left[\lambda_z^2 - 1\right]. \tag{25}$$

Figure 6 shows the predicted tensile stress for the armchair tubes at 300°K. Quite impressively, the tensile stress calculations based on the hyperelasticity model appear almost linearly dependent on

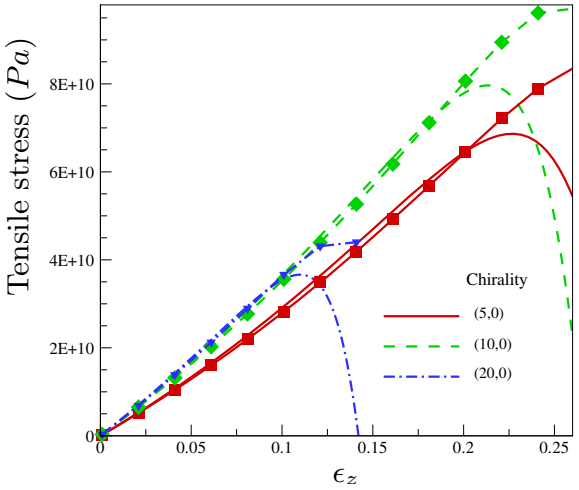

Figure 7: Tensile stresses prediction by the linear elasticity model and the hyperelasticity model. The lines with symbols are from Ogden's model. Zigzag tubes.

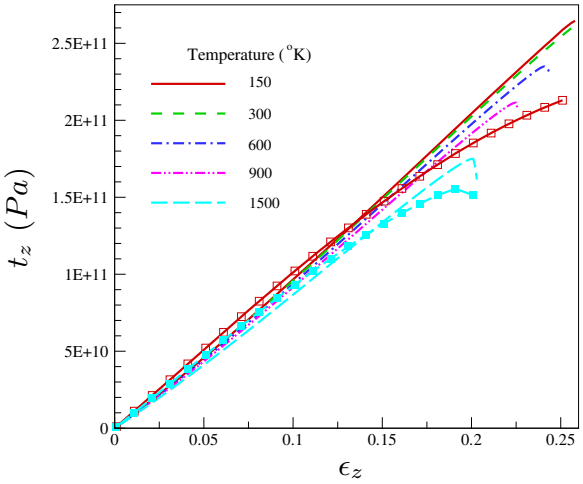

Figure 8: Temperature dependence of the tensile stresses for the hyperelasticity model. The tensile stresses σ_z for the linear elasticity model are plotted with symbols. (10,10).

tensile strains far beyond the critical point, while the linear elasticity model obviously reveals more nonlinearity in the stress responses. It can be seen that the hyperelasticity absorbs the nonlinearity into the model itself, while the linear elasticity characterizes the nonlinearity directly in its parameters. We also mark the stress level at the critical strain, which is about $50 \sim 60 GPa$, in excellent agreement with experimental observations. Overall, small tubes are slightly weaker than large tubes.

The predicted tensile stresses are shown in Figure 7 for the zigzag tubes. The linear stress responses are even more obvious for the hyperelasticity model, even valid for the early stage of failure. Comparing to the armchair tubes, the zigzag tubes are more ductile but less stronger. Figure 7 also shows that small tubes appear more ductile but weaker.

The dependence of the tensile stress on the temperature is shown in Figure 8 for the armchair tube (10,10). Again, for each individual temperature level studied, the tensile stresses appear linearly dependent on the applied strains, although the linearity become more attenuated for high temperatures and large applied strains. In accordance with Figure 5, the temperature dependence of the tensile stress is not very significant. In Figure 8, we only show the variations of the tensile stress σ_z for the linear elasticity model at $T = 150^o$K and 1500^oK. The linear elasticity model reveals more nonlinearity at high temperatures and high strains. Since no phase transformations or defects can be modeled herein, the high ductility for high temperatures as observed by Huang et al. (2006) cannot be predicted.

4 Summary

In summary, we propose an atom-based cell model for studying the mechanical behaviors of single wall carbon nanotubes. The finite temperature effects are also considered via the local harmonic approach. Also, a straightforward means to applying the Cauchy-Born rule to noncentrosymmetric atomic structures.

For the linear elasticity model, we show that strain energy can be fitted by cubic polynomials in two distinct stages, whereas the first stage corresponds to a linearly increasing tangent stiffness which ends up to the elastic limit, while the second stage corresponds to a linearly decreasing tangent stiffness. The tangent stiffness is on the order $1TPa$ for the armchair tubes, but reduced nearly by half for the zigzag tubes.

We propose to use Ogden's hyperelasticity model for describing the mechanical behaviors of SWNTs. Our results show that for large tubes, a constant μ is obtained for strains up to a critical point. Small tubes is shown to be more ductile but less stronger. Increasing temperature diminishes the elastic deformation. In describing the SWNT, we see that the hyperelasticity model contains the nonlinearity in itself, with a constant material parameter; while the linear elasticity model has to adopt a strain-dependent material parameter to reflect the inherent nonlinearity.

Acknowledgement: This work is supported by the National Science Foundation and the Army Research Office.

References

Arroyo, M.; Belytschko, T. (2004): Finite crystal elasticity of carbon nanotubes based on the exponential Cauchy-Born rule. *Physical Review B*, vol. 69, no. 11, pp. 115415.

Belytschko, T.; Xiao, S. P.; Schatz, G. C.; Ruoff, R. S. (2002): Atomistic simulations of nanotube fracture. *Physical Review B*, vol. 65, no. 23, pp. 235430.

Born, M.; Huang, K. (1954): *Dynamical theory of crystal lattices*. Oxford University Press, Oxford.

Brenner, D. W. (1990): Empirical potential for hydrocarbons for use in simulating the chemical vapor deposition of diamond films. *Physical Review B*, vol. 42, no. 15, pp. 9458–9471.

Cornwell, C. F.; Wille, L. T. (1997): Elastic properties of single-walled carbon nanotubes in compression. *Solid State Communications*, vol. 101, no. 8, pp. 555–558.

Demczyk, B. G.; Wang, Y. M.; Cumings, J.; Hetman, M.; Han, W.; Zettl, A.; Ritchie, R. O. (2002): Direct mechanical measurement of the tensile strength and elastic modulus of multiwalled carbon nanotubes. *Materials Science & Engineering A*, vol. 334, no. 1-2, pp. 173–178.

Gao, G.; Cagin, T.; Goddard, W. A. (1998): Energetics, structure, mechanical and vibrational properties of single-walled carbon nanotubes. *Nanotechnology*, vol. 9, no. 3, pp. 184–191.

Halicioglu, T. (1998): Stress calculations for carbon nanotubes. *Thin Solid Films*, vol. 312, no. 1-2, pp. 11–14.

Hernández, E.; Goze, C.; Bernier, P.; Rubio, A. (1998): Elastic properties of C and $B_xC_yN_z$ composite nanotubes. *Physical Review Letters*, vol. 80, no. 20, pp. 4502–4505.

Huang, J.; Chen, S.; Wang, Z.; Kempa, K.; Wang, Y.; Jo, S.; Chen, G.; Dresselhaus, M.; Ren, Z. (2006): Superplastic carbon nanotubes. *Nature*, vol. 439, no. 7074, pp. 281.

Krishnan, A.; Dujardin, E.; Ebbesen, T. W.; Yianilos, P. N.; Treacy, M. M. J. (1998): Young's modulus of single-walled nanotubes. *Physical Review B*, vol. 58, no. 20, pp. 14013–14019.

LeSar, R.; Najafabadi, R.; Srolovitz, D. J. (1989): Finite-temperature defect properties from free-energy minimization. *Physical Review Letters*, vol. 63, no. 6, pp. 624–627.

Li, F.; Cheng, H. M.; Bai, S.; Su, G.; Dresselhaus, M. S. (2000): Tensile strength of single-walled carbon nanotubes directly measured from their macroscopic ropes. *Applied Physics Letters*, vol. 77, no. 20, pp. 3161–3163.

Lourie, O.; Wagner, H. D. (1998): Evaluation of Young's modulus of carbon nanotubes by micro-Raman spectroscopy. *J. Mater. Res.*, vol. 13, no. 9, pp. 2418–2422.

Lu, J. P. (1997): Elastic properties of carbon nanotubes and nanoropes. *Physical Review Letters*, vol. 79, no. 7, pp. 1297–1300.

Nardelli, M. B.; Yakobson, B. I.; Bernholc, J. (1998): Brittle and ductile behavior in carbon nanotubes. *Physical Review Letters*, vol. 81, no. 21, pp. 4656–4659.

Natsuki, T.; Endo, M. (2005): Structural dependence of nonlinear elastic properties for carbon nanotubes using a continuum analysis. *Applied Physics A: Materials Science & Processing*, vol. 80, no. 7, pp. 1463–1468.

Ogden, R. W. (1984): *Non-linear elastic deformations*. Ellis Horwood Limited: Chichester, U. K.

Ozaki, T.; Iwasa, Y.; Mitani, T. (2000): Stiffness of single-walled carbon nanotubes under large strain. *Physical Review Letters*, vol. 84, no. 8, pp. 1712–1715.

Pan, Z. W.; Xie, S. S.; Lu, L.; Chang, B. H.; Sun, L. F.; Zhou, W. Y.; Wang, G.; Zhang, D. L. (1999): Tensile tests of ropes of very long aligned multiwall carbon nanotubes. *Applied Physics Letters*, vol. 74, no. 21, pp. 3152–3154.

Popov, V. N.; Van Doren, V. E.; Balkanski, M. (2000): Elastic properties of single-walled carbon nanotubes. *Physical Review B*, vol. 61, no. 4, pp. 3078–3084.

Robertson, D. H.; Brenner, D. W.; Mintmire, J. W. (1992): Energetics of nanoscale graphitic tubules. *Physical Review B*, vol. 45, no. 21, pp. 12592–12595.

Salvetat, J. P.; Briggs, G. A. D.; Bonard, J. M.; Bacsa, R. R.; Kulik, A. J.; Stöckli, T.; Burnham, N. A.; Forró, L. (1999): Elastic and shear moduli of single-walled carbon nanotube ropes. *Physical Review Letters*, vol. 82, no. 5, pp. 944–947.

Sears, A.; Batra, R. C. (2004): Macroscopic properties of carbon nanotubes from molecular-mechanics simulations. *Physical Review B*, vol. 69, no. 23, pp. 235406.

Tombler, T. W.; Zhou, C.; Alexseyev, L.; Kong, J.; Dai, H.; Liu, L.; Jayanthi, C. S.; Tang, M.; Wu, S. Y. (2000): Reversible electromechanical characteristics of carbon nanotubes under local-probe manipulation. *Nature*, vol. 405, no. 6788, pp. 769–72.

Treacy, M. M. J.; Ebbesen, T. W.; Gibson, J. M. (1996): Exceptionally high Young's modulus observed for individual carbon nanotubes. *Nature*, vol. 381, no. 6584, pp. 678–680.

Van Lier, G.; Van Alsenoy, C.; Van Doren, V.; Geerlings, P. (2000): Ab initio study of the elastic properties of single-walled carbon nanotubes and graphene. *Chem. Phys. Lett.*, vol. 326, pp. 181–185.

Wagner, H. D.; Lourie, O.; Feldman, Y.; Tenne, R. (1998): Stress-induced fragmentation of multiwall carbon nanotubes in a polymer matrix. *Applied Physics Letters*, vol. 72, no. 2, pp. 188–190.

Walters, D. A.; Ericson, L. M.; Casavant, M. J.; Liu, J.; Colbert, D. T.; Smith, K. A.; Smaller, R. E. (1999): Elastic strain of freely suspended single-wall carbon nanotube ropes. *Applied Physics Letters*, vol. 74, no. 25, pp. 3803–3805.

Wong, E. W.; Sheehan, P. E.; Lieber, C. M. (1997): Nanobeam mechanics: elasticity, strength, and toughness of nanorods and nanotubes. *Science*, vol. 277, no. 5334, pp. 1971–1975.

Xiao, T.; Liao, K. (2002): Nonlinear elastic properties of carbon nanotubes subjected to large axial deformations. *Physical Review B*, vol. 66, no. 15, pp. 153407.

Xiao, T.; Xu, X.; Liao, K. (2004): Characterization of nonlinear elasticity and elastic instability in single-walled carbon nanotubes. *Journal of Applied Physics*, vol. 95, no. 12, pp. 8145–8148.

Yakobson, B. I.; Brabec, C. J.; Bernholc, J. (1996): Nanomechanics of carbon tubes: instabilities beyond linear response. *Physical Review Letters*, vol. 76, no. 14, pp. 2511–2514.

Yao, N.; Lordi, V. (1998): Young's modulus of single-walled carbon nanotubes. *Journal of Applied Physics*, vol. 84, pp. 1939.

Yu, M. F.; Files, B. S.; Arepalli, S.; Ruoff, R. S. (2000): Tensile loading of ropes of single wall

carbon nanotubes and their mechanical properties. *Physical Review Letters*, vol. 84, no. 24, pp. 5552–5555.

Yu, M. F.; Lourie, O.; Dyer, M. J.; Moloni, K.; Kelly, T. F.; Ruoff, R. S. (2000): Strength and breaking mechanism of multiwalled carbon nanotubes under tensile load. *Science*, vol. 287, no. 5453, pp. 637–640.

Zhang, P.; Lammert, P. E.; Crespi, V. H. (1998): Plastic deformations of carbon nanotubes. *Physical Review Letters*, vol. 81, no. 24, pp. 5346–5349.

Zhou, G.; Duan, W.; Gu, B. (2001): First-principles study on morphology and mechanical properties of single-walled carbon nanotube. *Chemical Physics Letters*, vol. 333, no. 5, pp. 344–349.